

# Development and Verification of the Charring, Ablating Thermal Protection Implicit System Simulator

Adam J. Amar,<sup>\*</sup> Nathan Calvert,<sup>†</sup> and Benjamin S. Kirk<sup>‡</sup>

*NASA Lyndon B. Johnson Space Center*

*2101 NASA Parkway*

*Houston, TX, 77058, USA*

The development and verification of the Charring Ablating Thermal Protection Implicit System Solver (CATPISS) is presented. This work concentrates on the derivation and verification of the stationary grid terms in the equations that govern three-dimensional heat and mass transfer for charring thermal protection systems including pyrolysis gas flow through the porous char layer. The governing equations are discretized according to the Galerkin finite element method (FEM) with first and second order fully implicit time integrators. The governing equations are fully coupled and are solved in parallel via Newton's method, while the linear system is solved via the Generalized Minimum Residual method (GMRES). Verification results from exact solutions and Method of Manufactured Solutions (MMS) are presented to show spatial and temporal orders of accuracy as well as nonlinear convergence rates.

## I. Introduction

Cite Amar<sup>1</sup>

## II. Mathematical Model

### A. Governing Equations

The equations that govern the solid/gas system of the porous charring ablator include energy and mass conservation equations for the solid as well as the Navier-Stokes equations as applied to all of the gaseous species considered. In the general case, it is possible that the pyrolysis gases react with the remaining solid, or deposit residue (coke) on the solid, but these phenomena are neglected. Under the assumptions that the pyrolysis gas is in thermochemical equilibrium and the solid and gas are in thermal equilibrium, then the solid and gas energy equations for a stationary grid reduce to a mixture energy equation given by

$$\frac{\partial(\rho e_o)}{\partial t} = \nabla \cdot (\tilde{\mathbf{k}} \nabla T) - \nabla \cdot (\phi \rho_g h_{o_g} \mathbf{v}_g) + \dot{Q} \quad (1)$$

where  $\rho$ ,  $e_o$ ,  $\phi$ ,  $h_o$ ,  $\mathbf{v}$ , and  $\dot{Q}$  denote density, total energy, porosity, total enthalpy, velocity, and volumetric energy source respectively, and the subscript  $g$  denotes a quantity with respect to the pyrolysis gases. The velocity of the pyrolysis gases is governed by a porous flow law such as Darcy's law. Since ablators in general can be anisotropic materials, the thermal conductivity,  $\tilde{\mathbf{k}}$ , is a second order tensor. The solid mass conservation equation is simply

$$\frac{\partial \rho_s}{\partial t} = \dot{m}_s \quad (2)$$

If it is assumed that all solid decomposition results in pyrolysis gas generation, the gases are free to flow through the porous medium, and the gases occupy all of the pore space, then the gas mass conservation equation is given by

$$\frac{\partial(\phi \rho_g)}{\partial t} = -\dot{m}_s - \nabla \cdot (\phi \rho_g \mathbf{v}_g) \quad (3)$$

<sup>\*</sup>Applied Aeroscience and CFD Branch, Mail Code EG3, Member AIAA.

<sup>†</sup>Applied Aeroscience and CFD Branch, Mail Code EG3, Member AIAA.

<sup>‡</sup>Applied Aeroscience and CFD Branch, Mail Code EG3, Member AIAA.

Before manipulating the governing equations to yield a form suitable for implementation in a finite-element framework, it is first necessary to discuss the material model that will characterize the two-phase system.

## B. Material Model

In order to sufficiently explain the governing equations and boundary conditions, it is important to understand the material model used to characterize the state of the solid/gas mixture. It is assumed that all the pores are interconnected, and therefore pyrolysis gases occupy all of the pore space and are free to flow through it. Consequently, the density of the solid/gas mixture is described by

$$\rho = \phi\rho_g + \rho_s \quad (4)$$

where the solid density is a bulk density, the gas density is a density with respect to the space the gas occupies (pore space), and the porosity is equal to the gas volume fraction. In terms of units, Eq. 4 can be expressed as

$$\frac{\overbrace{[\text{total mass}]}^{\rho}}{[\text{total vol}]} = \frac{\overbrace{[\text{pore vol}]}^{\phi}}{[\text{total vol}]} \frac{\overbrace{[\text{gas mass}]}^{\rho_g}}{[\text{pore vol}]} + \frac{\overbrace{[\text{solid mass}]}^{\rho_s}}{[\text{total vol}]} \quad (5)$$

It is assumed that the thermodynamic state of the pyrolysis gases can be described as a mixture of perfect gases, and that the solid and gas phases are in thermal equilibrium resulting in

$$T_g = T_s = T \quad (6)$$

$$P = f(\rho_g, T) \quad (7)$$

where the equation of state and all relationships describing the thermochemical state of the gas are dictated by an external equilibrium chemistry module such as Cantera, CEA, MUTATION, etc. During the code development effort, Cantera has been used to provide the thermochemical state of the gas.

The solid material model adopted in this study is similar to the model developed by Moyer and Rindal (need citation) but has been expanded to include an arbitrary number of components,  $nc$ . The solid bulk density is given by

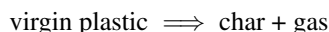
$$\rho_s = \sum_{i=1}^{nc} \Gamma_i \rho_i \quad (8)$$

where  $\Gamma_i$  is the volume fraction of the  $i^{th}$  component in the virgin composite and is therefore constant. The units associated with the solid bulk density model in Eq. 8 are

$$\frac{\overbrace{[\text{solid mass}]}^{\rho_s}}{[\text{total vol}]} = \sum_{i=1}^{nc} \frac{\overbrace{[\text{initial vol of } i^{th} \text{ comp.}]}}{[\text{total vol}]} \frac{\overbrace{[\text{mass of } i^{th} \text{ comp.}]}}{[\text{initial vol of } i^{th} \text{ comp.}]} \quad (9)$$

It is assumed that the solid does not change volume due to thermal expansion, and therefore the total volume is constant. It is important to note that the solid description in Eq. 8 is only a modeling assumption, and the solid is not truly comprised of  $nc$  components, species, or distinguishable materials. This modeling assumption comes as a result of decomposition data obtained from thermogravimetric analyses (TGA). It has been observed that phenolic resins undergo a two-stage decomposition process that can be appropriately captured by a two resin component model (need citation).

It is assumed that all decomposed solid mass results in gas mass generation, and the general model of the decomposition process is described by



This is a generalized description of the initial and final states of the system between which there are transitional states. The reaction is irreversible, and the pyrolysis gases are assumed to be in thermochemical equilibrium and do not react with the remaining solid in the pore space.

Taking the temporal derivative of Eq. 8 gives the solid decomposition rate in terms of component decomposition rates.

$$\frac{\partial \rho_s}{\partial t} = \sum_{i=1}^{nc} \Gamma_i \frac{\partial \rho_i}{\partial t} \quad (10)$$

It is assumed that the decomposition of each component can be described by an Arrhenius relationship of the form

$$\frac{\partial \rho_i}{\partial t} = -k_i \rho_{v_i} \left( \frac{\rho_i - \rho_{c_i}}{\rho_{v_i}} \right)^{\psi_i} e^{-E_i/RT} \text{ for } i = A, B, \text{ and } C \quad (11)$$

which applies at a constant spatial location (as apposed to a given node which can move during the solution process).

Since most thermophysical properties of the solid are only known for the virgin plastic and fully charred states, the intermediate solid is modeled as some interpolated state between virgin and char. This interpolated state is characterized by the extent of reaction ( $\beta$ ), or degree of char, given by

$$\beta = \frac{\rho_v - \rho_s}{\rho_v - \rho_c} \quad (12)$$

where the virgin and char bulk densities are known constants. It is evident that as the solid decomposes from virgin to char, the extent of reaction ranges from 0 to 1. The definition in Eq. 12 can be rearranged to more clearly describe the interpolated state.

$$\rho_s = (1 - \beta) \rho_v + \beta \rho_c \quad (13)$$

Although the virgin and char materials are not distinguishable entities within the intermediate solid, Eq. 13 reveals that the degree of char represents an effective char volume fraction within the solid (not in the solid/gas mixture). In a similar light, CMA defines an effective virgin mass fraction given by

$$y_v = \frac{\rho_v}{\rho_v - \rho_c} \left( 1 - \frac{\rho_c}{\rho_s} \right) \quad (14)$$

which can be related to the extent of reaction through

$$y_v = \frac{\rho_v}{\rho_s} (1 - \beta) \quad (15)$$

Similarly the char mass fraction is given by

$$y_c = 1 - y_v = \frac{\rho_c}{\rho_s} \beta \quad (16)$$

These effective parameters are used to determine several solid and mixture properties.

### C. Porous Flow Laws

Applying the Navier-Stokes momentum equations to flow through the char layer would require detailed knowledge of the pore structure, and that information is typically not known. Consequently, a porous flow law can be used as a simplified momentum equation. Porous flow laws typically require extra knowledge about the material beyond thermophysical properties. These properties include the porosity,  $\phi$ , and permeability,  $\kappa$  of the solid, as well as the viscosity,  $\mu$ , of the gas flowing through the porous medium. The porosity and permeability can be determined through material testing and is provided to *CATPISS* as a function of extent of reaction,  $\beta$ , which is given by Eq. 12.

#### 1. Darcy's Law

In 1856, Darcy (cite Darcy) published results from a series of experiments in which he determined how the volumetric flow rate,  $Q$ , of a laminar flowing fluid relates to the local pressure gradient within a fully saturated porous medium.

$$Q = -A \frac{\tilde{\kappa}}{\mu} \nabla P \quad (17)$$

where  $\tilde{\kappa}$  is the anisotropic permeability tensor. The superficial or filtration velocity is the volumetric flow rate averaged over the cross-sectional area of the medium and is given by

$$\mathbf{v}'_g = \frac{Q}{A} = -\frac{\tilde{\kappa}}{\mu} \nabla P \quad (18)$$

The average or seepage velocity of the fluid is the volumetric flow rate averaged over the cross-sectional area through which the fluid can flow (porous area) and is given by

$$\mathbf{v}_g = \frac{Q}{\phi A} = -\frac{\tilde{\kappa}}{\phi \mu} \nabla P \quad (19)$$

which assumes that the surface porosity is equal to the volumetric porosity. Darcy's law is valid for steady laminar flows with "sufficiently" low Reynolds numbers. While it is conceded that the pyrolysis gas flow within the porous ablator can not be adequately described by Darcy's law, it is being used for code development purposes due to its simplicity.

The seepage velocity can be used to determine the gas mass flux at any point within the medium according to

$$\dot{m}_g = (\phi \rho_g) \mathbf{v}_g = -(\phi \rho_g) \frac{\tilde{\boldsymbol{\kappa}}}{\phi \mu} \nabla P \quad (20)$$

Moving all terms to the LHS and simplifying gives

$$\phi \mu \mathbf{v}_g + \tilde{\boldsymbol{\kappa}} \nabla P = 0 \quad (21)$$

For the  $k^{th}$  dimension we have

$$\phi \mu (v_g)_k + \tilde{\boldsymbol{\kappa}}_k \cdot \nabla P = 0 \quad (22)$$

where  $\tilde{\boldsymbol{\kappa}}_k$  denotes the  $k^{th}$  row vector of the permeability tensor.

## D. Property Models

### 1. Internal Energy and Enthalpy

The total internal energy and of the system can be described by

$$\rho e_o = (1 - \beta) \rho_v e_v + \beta \rho_c e_c + \phi \rho_g e_{o_g} \quad (23)$$

where

$$e_{v/c} = h_{v/c} = h_{v/c}^o + \int_{T_o}^T C_{p_{v/c}}(T') dT' \quad (24)$$

and the total energy of the gas is

$$e_{o_g} = e_g^o + \int_{T_o}^T C_{v_g}(T') dT' + \frac{1}{2} (\mathbf{v}_g \cdot \mathbf{v}_g) \quad (25)$$

Similarly, the total enthalpy of the gas is

$$h_{o_g} = h_g^o + \int_{T_o}^T C_{p_g}(T') dT' + \frac{1}{2} (\mathbf{v}_g \cdot \mathbf{v}_g) \quad (26)$$

### 2. Thermal Conductivity

The thermal conductivity is in general an anisotropic function of temperature. The thermal conductivity tensor is given by

$$\tilde{\mathbf{k}}(T) = \begin{bmatrix} k_{11}(T) & k_{12}(T) & k_{13}(T) \\ k_{21}(T) & k_{22}(T) & k_{23}(T) \\ k_{31}(T) & k_{32}(T) & k_{33}(T) \end{bmatrix} \quad (27)$$

where each component of the tensor can be an independent function of temperature. For materials with anisotropies not aligned with coordinate axes, an additional transformation matrix must be introduced to appropriately apply the model. The thermal conductivity of the mixture is assumed to be a mass weighted average of virgin char and gas.

$$k = \frac{(1 - \beta) \rho_v}{\rho} k_v + \frac{\beta \rho_c}{\rho} k_c + \frac{\phi \rho_g}{\rho} k_g \quad (28)$$

### 3. Permeability

The permeability is in general an anisotropic function of the extent of reaction defined by Eq. 12. The permeability tensor is given by

$$\tilde{\boldsymbol{\kappa}}(\beta) = \begin{bmatrix} \kappa_{11}(\beta) & \kappa_{12}(\beta) & \kappa_{13}(\beta) \\ \kappa_{21}(\beta) & \kappa_{22}(\beta) & \kappa_{23}(\beta) \\ \kappa_{31}(\beta) & \kappa_{32}(\beta) & \kappa_{33}(\beta) \end{bmatrix} \quad (29)$$

where each component of the tensor can be an independent function of extent of reaction. For materials with anisotropies not aligned with coordinate axes, an additional transformation matrix must be introduced to appropriately apply the model.

#### 4. Porosity

The porosity is in general a function of extent of reaction defined by Eq. 12 and represents the gas mass fraction since all of the pore space is assumed to be interconnected.

$$\phi = \phi(\beta) \quad (30)$$

#### 5. Emissivity and Absorptivity

The emissivity and absorptivity of the mixture are assumed to be equal to the emissivity and absorptivity of the solid. They are modeled similarly to the thermal conductivity while only taking the solid portion into account

$$\epsilon = \frac{(1-\beta)\rho_v}{\rho_s}\epsilon_v + \frac{\beta\rho_c}{\rho_s}\epsilon_c \quad (31)$$

and

$$\alpha = \frac{(1-\beta)\rho_v}{\rho_s}\alpha_v + \frac{\beta\rho_c}{\rho_s}\alpha_c \quad (32)$$

### E. Galerkin Weak Statement

Given the material model, the governing equations can be manipulated to give

$$\begin{aligned} \text{Energy: } \left[ \rho C_v - \rho_g^2 \frac{\partial \phi}{\partial T} \frac{\partial e_g}{\partial \rho_g} \right] \frac{\partial T}{\partial t} + \left[ \rho_g \frac{\partial e_g}{\partial \rho_g} + e_{o_g} \right] \frac{\partial(\phi \rho_g)}{\partial t} + (\phi \rho_g) \mathbf{v}_g \cdot \frac{\partial \mathbf{v}_g}{\partial t} + \bar{e} \frac{\partial \rho_s}{\partial t} \\ - \nabla \cdot (\tilde{\mathbf{k}} \nabla T) + \nabla \cdot (\phi \rho_g h_{o_g} \mathbf{v}_g) - \dot{Q} = 0 \end{aligned} \quad (33)$$

$$\text{Momentum: } \phi \mu (v_g)_k + \tilde{\kappa}_k \cdot \nabla P = 0 \text{ for } k = 1 \dots \# \text{ dim} \quad (34)$$

$$\text{Solid Mass: } \frac{\partial \rho_s}{\partial t} - \dot{m}_s = 0 \quad (35)$$

and

$$\text{Gas Mass: } \frac{\partial(\phi \rho_g)}{\partial t} + \frac{\partial \rho_s}{\partial t} + \nabla \cdot (\phi \rho_g \mathbf{v}_g) = 0 \quad (36)$$

where

$$\rho C_v = (1-\beta)\rho_v C_{v_v} + \beta\rho_c C_{v_c} + \phi\rho_g C_{v_g} \quad (37)$$

and

$$\bar{e} = \frac{\rho_v e_v - \rho_c e_c}{\rho_v - \rho_c} \quad (38)$$

and

$$h_{o_g} = h_g(\rho_g, T) + \frac{\mathbf{v}_g \cdot \mathbf{v}_g}{2} \quad (39)$$

Since the model equation for  $\dot{m}_s$  is known, the solid mass conservation equation (Eq. 35) will be substituted into the energy and gas mass conservation equations. Consequently, the solution procedure will be to solve for the temperature, velocity, and gas density fields through integration of the PDEs given in Eqs. 33, 34, and 36 while the solid density will be treated as a nonlinearity, and the resulting ODE governing the solid density evolution will be numerically integrated.

#### 1. Energy Equation

A Galerkin weak statement can be developed for the energy equation (Eq. 33) by first multiplying it by a suitable test function,  $v$ , and integrating over the domain  $\Omega$  while integrating the 5<sup>th</sup> and 6<sup>th</sup> terms by parts to give the natural

boundary condition terms.

$$\begin{aligned} \int_{\Omega} \left[ v \left( \rho C_v - \rho_g^2 \frac{\partial \phi}{\partial T} \frac{\partial e_g}{\partial \rho_g} \right) \frac{\partial T}{\partial t} + v \bar{e} \dot{m}_s + v \left( \rho_g \frac{\partial e_g}{\partial \rho_g} + e_{o_g} \right) \frac{\partial (\phi \rho_g)}{\partial t} \right] d\Omega \\ + \int_{\Omega} \left[ \sum_{k=1}^{\# \text{dim}} v (\phi \rho_g) (v_g)_k \frac{\partial (v_g)_k}{\partial t} + \nabla v \cdot (\tilde{\mathbf{k}} \nabla T) - \nabla v \cdot (\phi \rho_g h_{o_g} \mathbf{v}_g) - v \dot{Q} \right] d\Omega \\ + \oint_{\Gamma} (v h_{o_g} \dot{m}_w + v \dot{q}_w) d\Gamma = 0 \quad \forall v \in H_0^1 \end{aligned} \quad (40)$$

where the boundary (wall) mass flux is

$$\dot{m}_w = (\phi \rho_g) \mathbf{v}_g \cdot \hat{\mathbf{n}} \quad (41)$$

and the boundary heat flux is

$$\dot{q}_w = -\tilde{\mathbf{k}} \nabla T \cdot \hat{\mathbf{n}} \quad (42)$$

## 2. Momentum Equations

For the  $k^{\text{th}}$  momentum equation we again multiply by a suitable test function,  $v$ , and integrate over the domain

$$\int_{\Omega} v \phi \mu (v_g)_k d\Omega + \int_{\Omega} v \tilde{\mathbf{k}}_k \cdot \nabla P d\Omega = 0 \quad \forall v \in H_0^1 \quad (43)$$

Since the porous flow law is simply a constraint equation, there is no need to integrate by parts to develop natural boundary condition terms. While it is recognized that the chain rule could be applied to the pressure gradient term to recast it in terms of independent variables, for simplicity it will be assumed that the pressure gradient at the quadrature points can be calculated according the local shape function and nodal pressure values.

## 3. Gas Mass Conservation Equation

Likewise, a Galerkin weak statement can be developed for the gas mass conservation equation (Eq. 36). Again, the equation will be multiplied by a suitable test function,  $v$ , and integrated over the domain  $\Omega$  while integrating the  $3^{\text{rd}}$  term by parts to give the natural boundary condition term.

$$\int_{\Omega} \left( \frac{\partial (\phi \rho_g)}{\partial t} v - \nabla v \cdot (\phi \rho_g \mathbf{v}_g) + \dot{m}_s v \right) d\Omega + \oint_{\Gamma} \dot{m}_w v d\Gamma = 0 \quad \forall v \in H_0^1 \quad (44)$$

During the development of CATPISS, it was observed that the hyperbolic nature of the gas continuity equation led to numerical instabilities during the solution procedure. Consequently, numerical dissipation or stabilization is required to solve the equation system. For the current work, the SUPG (Streamwise Upwind Petrov-Galerkin) stabilization technique has been implemented. The primary advantage of using a stabilization technique over simpler numerical dissipation techniques is that the solution to the stabilized system is consistent, meaning that the solution to the stabilized system still satisfies the original PDEs. Adding the SUPG terms to the gas mass conservation equations gives

$$\begin{aligned} \int_{\Omega} \left( \frac{\partial (\phi \rho_g)}{\partial t} v - \nabla v \cdot (\phi \rho_g \mathbf{v}_g) + \dot{m}_s v \right) d\Omega + \oint_{\Gamma} \dot{m}_w v d\Gamma \\ + \sum_{e=1}^{\# \text{elem}} \int_{\Omega_e} \tau \mathbf{v}_g \cdot \nabla v \left( \frac{\partial (\phi \rho_g)}{\partial t} + \dot{m}_s + \nabla \cdot (\phi \rho_g \mathbf{v}_g) \right) d\Omega_e = 0 \quad \forall v \in H_0^1 \end{aligned} \quad (45)$$

where  $\tau$  is the SUPG parameter of intrinsic time scales and is typically based on the element Reynolds number or element Peclet number. Expanding the last term gives

$$\begin{aligned} \int_{\Omega} \left( \frac{\partial (\phi \rho_g)}{\partial t} v - \nabla v \cdot (\phi \rho_g \mathbf{v}_g) + \dot{m}_s v \right) d\Omega + \oint_{\Gamma} \dot{m}_w v d\Gamma \\ + \sum_{e=1}^{\# \text{elem}} \int_{\Omega_e} \tau \mathbf{v}_g \cdot \nabla v \left( \frac{\partial (\phi \rho_g)}{\partial t} + \dot{m}_s + (\phi \rho_g) \nabla \cdot \mathbf{v}_g + \mathbf{v}_g \cdot \nabla (\phi \rho_g) \right) d\Omega_e = 0 \quad \forall v \in H_0^1 \end{aligned} \quad (46)$$

## E. Finite Element Formulation

Eqs. 40, 43, and 46 can be discretized by expanding the independent variables and test functions in terms of a finite dimensional basis

$$T_h(\mathbf{x}) = \sum_{j=1}^{\# \text{ nodes}} T_j \psi_j(\mathbf{x}) \quad (47)$$

$$(\phi \rho_g)_h(\mathbf{x}) = \sum_{j=1}^{\# \text{ nodes}} (\phi \rho_g)_j \psi_j(\mathbf{x}) \quad (48)$$

$$[(v_g)_k]_h(\mathbf{x}) = \sum_{j=1}^{\# \text{ nodes}} [(v_g)_k]_j \psi_j(\mathbf{x}) \quad (49)$$

$$\nabla P_h(\mathbf{x}) = \sum_{j=1}^{\# \text{ nodes}} P_j \nabla \psi_j(\mathbf{x}) \quad (50)$$

$$v_h(\mathbf{x}) = \sum_{i=1}^{\# \text{ nodes}} v_i \psi_i(\mathbf{x}) \quad (51)$$

where the subscript  $h$  is introduced to denote a finite dimensional approximation. Since the unknowns are no longer functions of  $\mathbf{x}$ , the PDE system reduces to an ODE system in which the temporal derivatives can be defined as

$$\frac{\partial T_h}{\partial t} = \sum_{j=1}^{\# \text{ nodes}} \dot{T}_j \psi_j(\mathbf{x}) \quad \text{where } \dot{T}_j = \frac{d}{dt}(T_j) \quad (52)$$

$$\frac{\partial (\phi \rho_g)_h}{\partial t} = \sum_{j=1}^{\# \text{ nodes}} (\dot{\phi \rho_g})_j \psi_j(\mathbf{x}) \quad \text{where } (\dot{\phi \rho_g})_j = \frac{d}{dt}(\phi \rho_g)_j \quad (53)$$

$$\frac{\partial [(v_g)_k]_h}{\partial t} = \sum_{j=1}^{\# \text{ nodes}} [\dot{(v_g)_k}]_j \psi_j(\mathbf{x}) \quad \text{where } [\dot{(v_g)_k}]_j = \frac{d}{dt}([\dot{(v_g)_k}]_j) \quad (54)$$

Since the equation system should be satisfied for all combinations of nodal shape function coefficients,  $v_i$ , their choice is arbitrary as long as a unique combination is chosen for each node. For the  $l^{\text{th}}$  nodal equation  $v_i = 1$  for  $i = l$  and  $v_i = 0$  for  $i \neq l$ . Consequently, Eqs. 40, 43, and 46 can now become

$$\begin{aligned} & \sum_{j=1}^{\# \text{ nodes}} \dot{T}_j \int_{\Omega} \left[ \rho C_v - \rho_g^2 \frac{\partial \phi}{\partial T} \frac{\partial e_g}{\partial \rho_g} \right] \psi_i \psi_j d\Omega + \sum_{j=1}^{\# \text{ nodes}} (\dot{\phi \rho_g})_j \int_{\Omega} \left[ \rho_g \frac{\partial e_g}{\partial \rho_g} + e_{o_g} \right] \psi_i \psi_j d\Omega \\ & + \sum_{k=1}^{\# \text{ dim}} \sum_{j=1}^{\# \text{ nodes}} [(\dot{v_g})_k]_j \int_{\Omega} (\phi \rho_g) (v_g)_k \psi_i \psi_j d\Omega + \sum_{j=1}^{\# \text{ nodes}} T_j \int_{\Omega} \nabla \psi_i \cdot \tilde{\mathbf{k}} \nabla \psi_j d\Omega \\ & - \sum_{j=1}^{\# \text{ nodes}} (\phi \rho_g)_j \int_{\Omega} h_{o_g} \psi_j \nabla \psi_i \cdot \mathbf{v}_g d\Omega + \int_{\Gamma} \psi_i q_w d\Gamma + \int_{\Gamma} \psi_i h_{o_g} \dot{m}_w d\Gamma + \int_{\Omega} \psi_i (\bar{e} \dot{m}_s - \dot{Q}) d\Omega = 0 \end{aligned} \quad (55)$$

$$\sum_{j=1}^{\# \text{ nodes}} [(\dot{v_g})_k]_j \int_{\Omega} \phi \mu \psi_i \psi_j d\Omega + \int_{\Omega} \psi_i \tilde{\mathbf{k}}_k \cdot \nabla P d\Omega = 0 \quad (56)$$

and

$$\begin{aligned}
& \sum_{j=1}^{\# \text{ nodes}} (\dot{\phi} \rho_g)_j \int_{\Omega} \psi_i \psi_j d\Omega - \sum_{j=1}^{\# \text{ nodes}} (\phi \rho_g)_j \int_{\Omega} \nabla \psi_i \cdot \psi_j \mathbf{v}_g d\Omega + \int_{\Gamma} \psi_i \dot{m}_w d\Gamma + \int_{\Omega} \psi_i \dot{m}_s d\Omega \\
& + \sum_{j=1}^{\# \text{ nodes}} (\dot{\phi} \rho_g)_j \sum_{e=1}^{\# \text{ elem}} \int_{\Omega_e} \psi_j \tau \mathbf{v}_g \cdot \nabla \psi_i d\Omega_e + \sum_{j=1}^{\# \text{ nodes}} (\phi \rho_g)_j \sum_{e=1}^{\# \text{ elem}} \int_{\Omega_e} \tau \mathbf{v}_g \cdot \nabla \psi_i (\psi_j \nabla \cdot \mathbf{v}_g) d\Omega_e \\
& + \sum_{j=1}^{\# \text{ nodes}} (\phi \rho_g)_j \sum_{e=1}^{\# \text{ elem}} \int_{\Omega_e} \tau \mathbf{v}_g \cdot \nabla \psi_i (\mathbf{v}_g \cdot \nabla \psi_j) d\Omega_e + \sum_{e=1}^{\# \text{ elem}} \int_{\Omega_e} \dot{m}_s \tau \mathbf{v}_g \cdot \nabla \psi_i d\Omega_e = 0
\end{aligned} \tag{57}$$

for  $i = 1, 2, \dots, \# \text{ nodes}$ . These can more concisely be written as

$$\sum_{j=1}^{\# \text{ nodes}} \left[ \dot{T}_j M_{ij}^{T,T} + (\dot{\phi} \rho_g)_j M_{ij}^{T,\rho} + \sum_{k=1}^{\# \text{ dim}} [(v_g)_k]_j M_{ij}^{T,v} + T_j K_{ij}^{T,T} + (\phi \rho_g)_j K_{ij}^{T,\rho} \right] + F_i^T = 0 \tag{58}$$

$$\sum_{j=1}^{\# \text{ nodes}} [(v_g)_k]_j K_{ij}^{v,v} + F_{ik}^v = 0 \text{ for } k = 1 \dots \# \text{ dim} \tag{59}$$

$$\sum_{j=1}^{\# \text{ nodes}} \left[ (\dot{\phi} \rho_g)_j \left( M_{ij}^{\rho,\rho} + M_{ij}^{\rho,SUPG} \right) + (\phi \rho_g)_j \left( K_{ij}^{\rho,\rho} + K_{ij}^{\rho,SUPG} \right) \right] + F_i^{\rho} + F_i^{\rho,SUPG} = 0 \tag{60}$$

for  $i = 1, 2, \dots, \# \text{ nodes}$ . Where

$$M_{ij}^{T,T} = \int_{\Omega} \left[ \rho C_v - \rho_g^2 \frac{\partial \phi}{\partial T} \frac{\partial e_g}{\partial \rho_g} \right] \psi_i \psi_j d\Omega \tag{61}$$

$$M_{ij}^{T,\rho} = \int_{\Omega} \left[ \rho_g \frac{\partial e_g}{\partial \rho_g} + e_{o_g} \right] \psi_i \psi_j d\Omega \tag{62}$$

$$M_{ij}^{T,v} = \int_{\Omega} (\phi \rho_g) (v_g)_k \psi_i \psi_j d\Omega \tag{63}$$

$$K_{ij}^{T,T} = \int_{\Omega} \nabla \psi_i \cdot \tilde{\mathbf{k}} \nabla \psi_j d\Omega \tag{64}$$

$$K_{ij}^{T,\rho} = - \int_{\Omega} h_{o_g} \psi_j \nabla \psi_i \cdot \mathbf{v}_g d\Omega \tag{65}$$

$$F_i^T = \int_{\Omega} \psi_i (\bar{e} \dot{m}_s - \dot{Q}) d\Omega + \int_{\Gamma} \psi_i q_w d\Gamma + \int_{\Gamma} \psi_i h_{o_g} \dot{m}_w d\Gamma \tag{66}$$

$$K_{ij}^{v,v} = \int_{\Omega} \phi \mu \psi_i \psi_j d\Omega \tag{67}$$

$$F_{ik}^v = \int_{\Omega} \psi_i \tilde{\boldsymbol{\kappa}}_k \cdot \nabla P d\Omega \tag{68}$$

$$M_{ij}^{\rho,\rho} = \int_{\Omega} \psi_i \psi_j d\Omega \tag{69}$$

$$K_{ij}^{\rho,\rho} = - \int_{\Omega} \psi_j \nabla \psi_i \cdot \mathbf{v}_g d\Omega \tag{70}$$

$$M_{ij}^{\rho,SUPG} = \sum_{e=1}^{\# \text{ elem}} \int_{\Omega_e} \psi_j \tau \mathbf{v}_g \cdot \nabla \psi_i d\Omega_e \tag{71}$$

$$K_{ij}^{\rho,SUPG} = \sum_{e=1}^{\# \text{ elem}} \int_{\Omega_e} \tau \mathbf{v}_g \cdot \nabla \psi_i (\psi_j \nabla \cdot \mathbf{v}_g) d\Omega_e + \sum_{e=1}^{\# \text{ elem}} \int_{\Omega_e} \tau \mathbf{v}_g \cdot \nabla \psi_i (\mathbf{v}_g \cdot \nabla \psi_j) d\Omega_e \tag{72}$$



$$F_i^{\rho, SUPG} = \sum_{e=1}^{\# \text{ elem}} \int_{\Omega_e} \dot{m}_s \tau \mathbf{v}_g \cdot \nabla \psi_i d\Omega_e \quad (73)$$

$$F_i^{\rho} = \int_{\Gamma} \psi_i \dot{m}_w d\Gamma + \int_{\Omega} \psi_i \dot{m}_s d\Omega \quad (74)$$

## G. Time Discretization

The semidiscrete weak form of the system given by Eqs. 58 and 60 is discretized in time using backwards finite difference schemes. Both first and second-order accurate in time schemes may be derived from Taylor series expansions in time about  $\mathbf{U}_h(t_{n+1}) = \mathbf{U}_{n+1}$ :

$$\begin{aligned} \mathbf{U}_n &= \mathbf{U}_{n+1} + \frac{\partial \mathbf{U}_{n+1}}{\partial t} (t_n - t_{n+1}) + \frac{\partial^2 \mathbf{U}_{n+1}}{\partial t^2} \frac{(t_n - t_{n+1})^2}{2} + \mathcal{O}((t_n - t_{n+1})^3) \\ \mathbf{U}_{n-1} &= \mathbf{U}_{n+1} + \frac{\partial \mathbf{U}_{n+1}}{\partial t} (t_{n-1} - t_{n+1}) + \frac{\partial^2 \mathbf{U}_{n+1}}{\partial t^2} \frac{(t_{n-1} - t_{n+1})^2}{2} + \mathcal{O}((t_{n-1} - t_{n+1})^3) \end{aligned}$$

These expressions can be manipulated as in<sup>2,3</sup> to create difference formulas of the form

$$\frac{\partial \mathbf{U}_{n+1}}{\partial t} = \alpha_t \mathbf{U}_{n+1} + \beta_t \mathbf{U}_n + \gamma_t \mathbf{U}_{n-1} + \mathcal{O}(\Delta t_{n+1}^p) \quad (75)$$

to yield either a first or second-order accurate scheme. The weights  $\alpha_t$ ,  $\beta_t$ , and  $\gamma_t$  are given for  $p = 1$  and  $p = 2$  in Table 1.

**Table 1. First and second-order accurate time discretization coefficients.**

$p$	$\alpha_t$	$\beta_t$	$\gamma_t$
1	$\frac{1}{\Delta t_{n+1}}$	$\frac{-1}{\Delta t_{n+1}}$	0
2	$-\beta_t - \gamma_t$	$-\left[\frac{1}{\Delta t_{n+1}} + \frac{1}{\Delta t_n}\right]$	$\frac{\Delta t_{n+1}}{\Delta t_n(\Delta t_{n+1} + \Delta t_n)}$

The resulting equation system is

$$\begin{aligned} \sum_{j=1}^{\# \text{ nodes}} \left\{ \left( \alpha_t M_{ij}^{T,T} + K_{ij}^{T,T} \right) T_j^{n+1} + \left( \alpha_t M_{ij}^{T,\rho} + K_{ij}^{T,\rho} \right) (\phi \rho_g)_j^{n+1} + \sum_{k=1}^{\# \text{ dim}} \alpha_t M_{ij}^{T,v} [(v_g)_k]_j \right\} \\ + \sum_{j=1}^{\# \text{ nodes}} \left\{ \beta_t M_{ij}^{T,T} T_j^n + \beta_t M_{ij}^{T,\rho} (\phi \rho_g)_j^n + \sum_{k=1}^{\# \text{ dim}} \beta_t M_{ij}^{T,v} [(v_g)_k]_j \right\} \\ + \sum_{j=1}^{\# \text{ nodes}} \left\{ \gamma_t M_{ij}^{T,T} T_j^{n-1} + \gamma_t M_{ij}^{T,\rho} (\phi \rho_g)_j^{n-1} + \sum_{k=1}^{\# \text{ dim}} \gamma_t M_{ij}^{T,v} [(v_g)_k]_j \right\} + F_i^T = 0 = \mathcal{R}_i^T \quad (76) \end{aligned}$$

$$\sum_{j=1}^{\# \text{ nodes}} K_{ij}^{v,v} [(v_g)_k]_j^{n+1} + F_{ik}^v = 0 = \mathcal{R}_i^v \text{ for } k = 1 \dots \# \text{ dim} \quad (77)$$

$$\begin{aligned} \sum_{j=1}^{\# \text{ nodes}} \left\{ \left[ \alpha_t \left( M_{ij}^{\rho,\rho} + M_{ij}^{\rho, SUPG} \right) + K_{ij}^{\rho,\rho} + K_{ij}^{\rho, SUPG} \right] (\phi \rho_g)_j^{n+1} \right\} \\ + \sum_{j=1}^{\# \text{ nodes}} \left\{ \beta_t \left( M_{ij}^{\rho,\rho} + M_{ij}^{\rho, SUPG} \right) (\phi \rho_g)_j^n + \gamma_t \left( M_{ij}^{\rho,\rho} + M_{ij}^{\rho, SUPG} \right) (\phi \rho_g)_j^{n-1} \right\} \\ + F_i^{\rho} + F_i^{\rho, SUPG} = 0 = \mathcal{R}_i^{\rho} \quad (78) \end{aligned}$$

for  $i = 1, 2, \dots, \# \text{ nodes}$ , where  $\mathcal{R}_i$  denotes the  $i^{th}$  nonlinear nodal residual equations which is driven to machine zero during the iteration process. The integrals in Eqs. 61-74 are evaluated with  $T^{n+1}$ ,  $(\phi \rho_g)^{n+1}$ , and  $\mathbf{v}_g^{n+1}$ .

## H. Linearization

Through the iteration process the nodal residual equations in Eqs. 76, 77, and 78 will be driven to machine zero so that the governing equations are satisfied in a discrete sense. To aid in the iterative process, it is necessary to linearize the residual equations in iteration space. This will be done according to the familiar Taylor-series expansion

$$\mathcal{R}_i^{\nu+1} = \mathcal{R}_i^\nu + \sum_{j=1}^{\# \text{ nodes}} \left\{ \frac{\partial \mathcal{R}_i}{\partial T_j} \Big|^\nu \Delta T_j + \frac{\partial \mathcal{R}_i}{\partial (\phi \rho_g)_j} \Big|^\nu \Delta (\phi \rho_g)_j + \sum_{k=1}^{\# \text{ dim}} \frac{\partial \mathcal{R}_i}{\partial [(v_g)_k]_j} \Big|^\nu \Delta [(v_g)_k]_j \right\} + \text{higher order terms} \quad (79)$$

where the superscript  $\nu$  has been introduced to denote iteration level and

$$\Delta ()_j = ()_j^{\nu+1} - ()_j^\nu \quad (80)$$

Keep in mind that the Jacobian terms,  $\frac{\partial \mathcal{R}_i}{\partial ()_j}$ , are only nonzero if nodes  $i$  and  $j$  share an element.

Since the intent of *CATPISS* is to allow for easy addition of material models and porous flow laws, the Jacobians will not be derived analytically yet they will be calculated exactly (to machine precision) using the complex-step method. The implementation of the complex-step method does not disallow the use of analytically derived Jacobian terms (or some mix of the two), so these terms can be replaced with analytical expressions at a later date if desired.

The residuals can be expanded according to a Taylor-series expansion in independent variable space about a point  $[T, (\phi \rho_g), \mathbf{v}_g]$ . For example let's do the expansion in temperature space and take a complex step,  $i\Delta T$ .

$$\mathcal{R}[T + i\Delta T, (\phi \rho_g), \mathbf{v}_g] = \mathcal{R}[T, (\phi \rho_g), \mathbf{v}_g] + i \frac{\partial \mathcal{R}}{\partial T} (\Delta T) - \frac{1}{2} \frac{\partial^2 \mathcal{R}}{\partial T^2} (\Delta T)^2 - \frac{i}{6} \frac{\partial^3 \mathcal{R}}{\partial T^3} (\Delta T)^3 + \text{higher order terms} \quad (81)$$

Now looking at just the imaginary part and ignoring the higher order terms gives

$$\text{Im} \{ \mathcal{R}[T + i\Delta T, (\phi \rho_g), \mathbf{v}_g] \} = \frac{\partial \mathcal{R}}{\partial T} \Delta T - \frac{1}{6} \frac{\partial^3 \mathcal{R}}{\partial T^3} (\Delta T)^3 \quad (82)$$

Solving for the first derivative gives the Jacobian terms

$$\frac{\partial \mathcal{R}}{\partial T} = \frac{\text{Im} \{ \mathcal{R}[T + i\Delta T, (\phi \rho_g), \mathbf{v}_g] \}}{\Delta T} + \mathcal{O} [(\Delta T)^2] \quad (83)$$

This process can be repeated for each independent variable. The proper choice for the perturbation steps is not immediately obvious from looking at the equations. In general, the perturbation step should have some relationship to the order of magnitude of the independent variable.

$$\Delta () = r () \quad (84)$$

Taking advantage of the fact that the problem will be solved on a finite precision machine,  $r$  can be chosen so that the second order error terms in the Jacobian expressions are smaller the smallest orders represented in the first terms. Consequently, the derivatives will be accurate to machine precision. Having such a small step does not affect the division operation in the first term because multiplication/division operations simply result in an exponent shift. Choosing  $r = 10^{-16}$  for a double precision calculation will accomplish this.

For each node, the calculation of all of the Jacobian terms will require

$$[\# \text{ Residual Calcs}] = [1 + (\# \text{ other nodes on common elements})] \times [\# \text{ d.o.f.}]$$

complex residual calculations where # dof is the number of degrees of freedom, which is 2 for the current system. The scope of the residual recalculations can be reduced by only recalculating those terms that depend on the degree of freedom with the current complex perturbation. One fortuitous aspect of this method is that there is no separate residual calculation required for the unperturbed state. If only one independent variables is perturbed (use  $T$  for example), then the real part of Eq. 81 can be solved for the residual

$$\mathcal{R}[T, (\phi \rho_g), \mathbf{v}_g] = \text{Real} \{ \mathcal{R}[T + i\Delta T, (\phi \rho_g), \mathbf{v}_g] \} + \mathcal{O} [(\Delta T)^2] \quad (85)$$

Again since the independent variable perturbation has been chosen to be sufficiently small, the order of magnitude of the error terms is smaller than the smallest order represented in the complex-step residual calculation. This results in a residual calculation exact to machine precision.

The advantage of the complex-step method is in the development cost. The derivation, implementation, and debugging of analytical Jacobian terms can be time consuming. Plus, the addition and/or modification of models with the complex-step method can be accomplished with relative ease. The drawbacks are the extra time spent doing complex arithmetic, and the extra storage required for complex variables.

## I. Boundary Conditions

*CATPISS* can handle a rich suite of boundary conditions, including multiple flux type boundary conditions that can be summed over a given boundary. *CATPISS* currently accepts EXODUSII (reference) unstructured grid files including side set definitions for boundary conditions. In the current implementation, a side set can be thought of as a collection of one or more boundary conditions that is defined for each subdomain exterior boundary. For example, a subdomain exterior boundary may have a Dirichlet (specified temperature) condition (1 boundary condition) or an Neumann (specified flux) condition (1 boundary condition) imposed on it. Alternatively, the boundary could be exposed to a convective environment with shock-layer radiation and far-field reradiation (3 boundary conditions) at the same time. In addition, *CATPISS* has the ability to handle both constant and time-dependent boundary conditions each with their own input nomenclature. Internally, *CATPISS* converts constant boundary conditions to time-dependent conditions so that their application within the element assembly routines can use the same logic.

### 1. Specified Temperature

Dirichlet conditions and other conditions that require the substitution of a nodal residual equation with a boundary condition specific equation will be imposed via the penalty boundary method (PBM) (reference). With this method, the  $L_2$  projection of the residuals are added to the matrix. The projection is multiplied by some large factor so that, in floating point arithmetic, the existing (smaller) entries in the matrix and right-hand-side are effectively ignored. The boundary integral in the weak form becomes

$$\frac{1}{\epsilon} \int_{\Gamma} \psi_i \mathcal{R} d\Gamma = 0 \quad (86)$$

where  $\epsilon \ll 1$ . For the specified temperature condition, the residual equation is given by

$$\mathcal{R} = T_{spec} - T_h(\mathbf{x}) = 0 \quad (87)$$

where  $T_{spec}$  is the known specified temperature. Substituting in the definition of  $T_h(x)$  in the finite dimensional basis, Eq. 47, gives

$$\mathcal{R} = T_{spec} - \sum_{j=1}^{\# \text{ nodes}} T_j \psi_j(\mathbf{x}) = 0 \quad (88)$$

Substituting the residual definition into Eq. 86 gives the weak form of the discrete residual equations

$$\mathcal{R}_i = \frac{1}{\epsilon} \int_{\Gamma} \psi_i \left( T_{spec} - \sum_{j=1}^{\# \text{ nodes}} T_j \psi_j(\mathbf{x}) \right) d\Gamma = 0 \quad (89)$$

Employing a numerical integration technique, such as Gaussian quadrature, to evaluate the surface integral gives

$$\mathcal{R}_i = \frac{1}{\epsilon} \sum_{QP=1}^{\# \text{ QPs}} \left[ w \psi_i \left( T_{spec} - \sum_{j=1}^{\# \text{ nodes}} T_j \psi_j \right) \right] \Big|_{QP} \quad (90)$$

where  $QP$  denotes the quadrature point and  $w$  is the integration weight. Linearizing in iteration space according to a Taylor-series expansion while ignoring higher order terms gives

$$\mathcal{R}_i^{\nu+1} = \mathcal{R}_i^{\nu} + \sum_{j=1}^{\# \text{ nodes}} \left. \frac{\partial \mathcal{R}_i}{\partial T_j} \right|_{\nu} \Delta T_j \quad (91)$$

Differentiating Eq. 90 gives the Jacobian terms for the linear system

$$\frac{\partial \mathcal{R}_i}{\partial T_j} = -\frac{w}{\epsilon} \psi_i \psi_j \quad (92)$$

Given the ease of the Jacobian derivation, this boundary condition has been implemented using analytical Jacobians as opposed to using the complex perturbation approach.

## 2. Specified Heat Flux

The specified flux boundary condition is linear and requires no Jacobian contributions. The boundary heat flux term in Eq. 66 becomes

$$\int_{\Gamma} \psi_i q_w d\Gamma = - \int_{\Gamma} \psi_i q_{spec} d\Gamma \quad (93)$$

where  $q_{spec}$  is the known specified flux. Note that the sign change is intended to simplify usability. In the original PDE derivation, fluxes into the body were considered a negative quantity. So the sign change allows the user to input a positive heat flux when the intent is to put heat into the body. Introducing Gaussian quadrature for numerical integration gives

$$- \int_{\Gamma} \psi_i q_{spec} d\Gamma = \sum_{QP=1}^{\# \text{ QPs}} -w q_{spec} \psi_i \quad (94)$$

## 3. Convection

The convective heat flux is given by

$$q_{conv} = h (T_{rec} - T_w) \quad (95)$$

Substituting into Eq. 66 gives

$$\int_{\Gamma} \psi_i q_w d\Gamma = - \int_{\Gamma} \psi_i h (T_{rec} - T_w) d\Gamma \quad (96)$$

Introducing Gaussian quadrature for numerical integration and the finite dimensional basis representation of temperature gives

$$- \int_{\Gamma} \psi_i h (T_{rec} - T_w) d\Gamma = \sum_{QP=1}^{\# \text{ QPs}} \left[ -w \psi_i h \left( T_{rec} - \sum_{j=1}^{\# \text{ nodes}} T_j \psi_j(\mathbf{x}) \right) \right] \Big|_{QP} \quad (97)$$

The Jacobian contributions for the convective boundary condition are calculated using the complex perturbation method.

## 4. (

Specified Pressure) Since the independent variables in the linear system are temperature and gas density, the specified pressure condition is nonlinear and must be applied through the PBM method to replace the appropriate gas density residual equations in the linear system. An additional complication is introduced because the energy equation requires a mass flux at the surface to complete the energy balance. Consequently the surface mass flux must be backed out from the known data. Before boundary conditions are applied, but after the

# III. Governing Equation Derivation

## A. Energy Equation

The thermochemical equilibrium energy equation describing the charring porous ablator with pyrolysis gas flow on a stationary grid is

$$\frac{\partial(\rho e_o)}{\partial t} - \nabla \cdot (\tilde{\mathbf{k}} \nabla T) + \nabla \cdot (\phi \rho_g h_{o_g} \mathbf{v}_g) - \dot{Q} = 0 \quad (98)$$

where

$$\rho e_o = (1 - \beta) \rho_v e_v + \beta \rho_c e_c + \phi \rho_g e_{o_g} \quad (99)$$

The virgin and char internal energies are equal to the virgin and char enthalpies respectively and are given by

$$e_{v/c} = h_{v/c} = h_{v/c}^o + \int_{T^o}^T C_{v_{v/c}}(T') dT' \quad (100)$$

and the gas total energy is given by

$$e_{o_g} = e_g(\rho_g, T) + \frac{\mathbf{v}_g \cdot \mathbf{v}_g}{2} \quad (101)$$

$\beta$  is called the “degree of char” or “extent of reaction” and is defined to be

$$\beta = \frac{\rho_v - \rho_s}{\rho_v - \rho_c} \quad (102)$$

which represents the char volume fraction within the virgin/char mixture. While there are no distinct virgin and char materials in the solid, the extent of reaction is introduced as a modeling assumption to weight thermal properties in the decomposition region since only virgin and char properties are known. The extent of reaction definition can be rearranged to give the solid density

$$\rho_s = (1 - \beta) \rho_v + \beta \rho_c \quad (103)$$

and the total mixture density is given by

$$\rho = \phi \rho_g + \rho_s \quad (104)$$

Using the chain rule to evaluate the temporal derivative in the energy equation we have

$$\frac{\partial(\rho e_o)}{\partial t} = (1 - \beta) \rho_v C_{v_v} \frac{\partial T}{\partial t} + \beta \rho_c C_{v_c} \frac{\partial T}{\partial t} + \phi \rho_g \frac{\partial e_{o_g}}{\partial t} + e_{o_g} \frac{\partial(\phi \rho_g)}{\partial t} + \bar{e} \frac{\partial \rho_s}{\partial t} \quad (105)$$

where

$$\bar{e} = \frac{\rho_v e_v - \rho_c e_c}{\rho_v - \rho_c} \quad (106)$$

Concentrating now on the temporal derivative of the gas total energy we have

$$\frac{\partial e_{o_g}}{\partial t} = \frac{\partial e_g}{\partial t} + \mathbf{v}_g \cdot \frac{\partial \mathbf{v}_g}{\partial t} \quad (107)$$

where

$$\frac{\partial e_g}{\partial t} = C_{v_g} \frac{\partial T}{\partial t} + \frac{\partial e_g}{\partial \rho_g} \frac{\partial \rho_g}{\partial t} \quad (108)$$

In the solution process, the gas density is a nonlinear function of both  $T$  and  $(\phi \rho_g)$  given by

$$\rho_g = \frac{(\phi \rho_g)}{\phi} \quad (109)$$

and consequently

$$\frac{\partial \rho_g}{\partial t} = \frac{\partial \rho_g}{\partial(\phi \rho_g)} \frac{\partial(\phi \rho_g)}{\partial t} + \frac{\partial \rho_g}{\partial T} \frac{\partial T}{\partial t} \quad (110)$$

Performing the necessary differentiation gives

$$\frac{\partial \rho_g}{\partial(\phi \rho_g)} = \frac{1}{\phi} \quad (111)$$

and

$$\frac{\partial \rho_g}{\partial T} = -\frac{(\phi \rho_g)}{\phi^2} \frac{\partial \phi}{\partial T} \quad (112)$$

Substituting into Eq. 107 and collecting terms gives

$$\frac{\partial e_{o_g}}{\partial t} = \left( C_{v_g} - \frac{(\phi \rho_g)}{\phi^2} \frac{\partial \phi}{\partial T} \frac{\partial e_g}{\partial \rho_g} \right) \frac{\partial T}{\partial t} + \frac{1}{\phi} \frac{\partial e_g}{\partial \rho_g} \frac{\partial(\phi \rho_g)}{\partial t} + \mathbf{v}_g \cdot \frac{\partial \mathbf{v}_g}{\partial t} \quad (113)$$

Substituting back into Eq. 105 gives

$$\begin{aligned} \frac{\partial(\rho e_{o_g})}{\partial t} = & \left[ (1 - \beta) \rho_v C_{v_v} + \beta \rho_c C_{v_c} + (\phi \rho_g) \left( C_{v_g} - \frac{(\phi \rho_g)}{\phi^2} \frac{\partial \phi}{\partial T} \frac{\partial e_g}{\partial \rho_g} \right) \right] \frac{\partial T}{\partial t} \\ & + \left[ \frac{(\phi \rho_g)}{\phi} \frac{\partial e_g}{\partial \rho_g} + e_{o_g} \right] \frac{\partial(\phi \rho_g)}{\partial t} \\ & + (\phi \rho_g) \mathbf{v}_g \cdot \frac{\partial \mathbf{v}_g}{\partial t} + \bar{e} \frac{\partial \rho_s}{\partial t} \end{aligned} \quad (114)$$

Further simplifying gives

$$\frac{\partial(\rho e_{o_g})}{\partial t} = \left[ \rho C_v - \rho_g^2 \frac{\partial \phi}{\partial T} \frac{\partial e_g}{\partial \rho_g} \right] \frac{\partial T}{\partial t} + \left[ \rho_g \frac{\partial e_g}{\partial \rho_g} + e_{o_g} \right] \frac{\partial(\phi \rho_g)}{\partial t} + (\phi \rho_g) \mathbf{v}_g \cdot \frac{\partial \mathbf{v}_g}{\partial t} + \bar{e} \frac{\partial \rho_s}{\partial t} \quad (115)$$

where

$$\rho C_v = (1 - \beta) \rho_v C_{v_v} + \beta \rho_c C_{v_c} + \phi \rho_g C_{v_g} \quad (116)$$

In summary, the final form of the energy equation is

$$\begin{aligned} \left[ \rho C_v - \rho_g^2 \frac{\partial \phi}{\partial T} \frac{\partial e_g}{\partial \rho_g} \right] \frac{\partial T}{\partial t} + \left[ \rho_g \frac{\partial e_g}{\partial \rho_g} + e_{o_g} \right] \frac{\partial(\phi \rho_g)}{\partial t} + (\phi \rho_g) \mathbf{v}_g \cdot \frac{\partial \mathbf{v}_g}{\partial t} + \bar{e} \frac{\partial \rho_s}{\partial t} \\ - \nabla \cdot (\tilde{\mathbf{k}} \nabla T) + \nabla \cdot (\phi \rho_g h_{o_g} \mathbf{v}_g) - \dot{Q} = 0 \end{aligned} \quad (117)$$

where

$$\rho C_v = (1 - \beta) \rho_v C_{v_v} + \beta \rho_c C_{v_c} + \phi \rho_g C_{v_g} \quad (118)$$

$$h_{o_g} = h_g(\rho_g, T) + \frac{\mathbf{v}_g \cdot \mathbf{v}_g}{2} \quad (119)$$

and

$$\bar{e} = \frac{\rho_v e_v - \rho_c e_c}{\rho_v - \rho_c} \quad (120)$$

## B. Momentum Equations

The momentum equations will be simplified through the use of porous flow laws. There are several different options, but Darcy's law will be used for initial development purposes.

### 1. Darcy's Law

Darcy's law was initially empirically developed through porous flow experiments by Darcy, and it has since been analytically derived directly from the Navier-Stokes equations. Darcy's law governs the volumetric flow rate of a steady incompressible low Reynolds number laminar fluid flow through a uniform porous medium. While it is recognized that the pyrolysis gas flow through the char layer is neither steady nor incompressible, Darcy's law is the simplest porous flow law and will be used for initial development. More appropriate momentum equation models can be implemented in the future.

The volumetric flow rate,  $\mathbf{Q}$ , is given by

$$\mathbf{Q} = -A \frac{\tilde{\kappa}}{\mu} \nabla P \quad (121)$$

Consequently, the mass flow rate is

$$\rho_g \mathbf{Q} = -\rho_g A \frac{\tilde{\kappa}}{\mu} \nabla P \quad (122)$$

Averaging the mass flow rate over the sample area through which it flows gives the mass flux

$$\rho_g \mathbf{v}'_g = -\rho_g \frac{\tilde{\kappa}}{\mu} \nabla P \quad (123)$$

where  $\mathbf{v}'_g$  is the superficial or filtration velocity of the gas. If it is assumed that the surface porosity is equal to the volumetric porosity, then the average velocity (or pore velocity) of the gas is given by

$$\mathbf{v}_g = \frac{\mathbf{v}'_g}{\phi} \quad (124)$$

The mass flux can now be restated in terms of the gas velocity

$$\phi \rho_g \mathbf{v}_g = -\rho_g \frac{\tilde{\kappa}}{\mu} \nabla P \quad (125)$$

There will be one equation in the PDE system for each velocity component

$$\phi \mu (v_g)_k + \tilde{\kappa}_k \cdot \nabla P = 0 \quad (126)$$

where  $k$  represents the Cartesian dimension and  $\tilde{\kappa}_k$  is the  $k^{\text{th}}$  row vector of the permeability tensor

$$\tilde{\kappa}(\beta) = \begin{bmatrix} \kappa_{11}(\beta) & \kappa_{12}(\beta) & \kappa_{13}(\beta) \\ \kappa_{21}(\beta) & \kappa_{22}(\beta) & \kappa_{23}(\beta) \\ \kappa_{31}(\beta) & \kappa_{32}(\beta) & \kappa_{33}(\beta) \end{bmatrix} \quad (127)$$

where each component is a function of the extent of reaction.

### C. Gas Mass Conservation Equation

$$\frac{\partial \phi \rho_g}{\partial t} = -\dot{m}_s - \nabla \cdot (\phi \rho_g \mathbf{v}_g) \quad (128)$$

## IV. Verification

Multiple levels of verification are performed to ensure that *CATPISS* correctly solves the governing equations over a variety of geometries and flow conditions. First, temperature profiles are obtained for analytic solutions to the one-dimensional heat equation for several different boundary conditions. Next, multidimensional solutions are calculated for the convective boundary condition on a cube, cylinder and sphere then compared with the temperature distributions estimated with *CATPISS*. Second-order convergence of the spatial discretization routine in *CATPISS* is demonstrated in the normalized error between the exact solution and code output as the grid is refined. Lastly, the method of manufactured solutions provides general evidence that the code accurately recreates a preconceived temperature profile as defined by a source term in the governing equation.

### A. One-dimensional Heat Equation

The one-dimensional heat equation describes the distribution and evolution of temperature in a medium

$$\rho C_v \frac{\partial T}{\partial t} = k \frac{\partial^2 T}{\partial x^2} \quad 0 \leq x \leq L \quad (129)$$

where  $\rho$  is the density of the material,  $C_v$  is the specific heat at constant volume and  $k$  is the thermal conductivity. The heat equation is of particular interest in this study since it is in the same form as the ablation governing equations and has exact solutions for a myriad of boundary conditions. A comparison of the temperature profile given by the exact solution and simulated numerically by *CATPISS* is presented for a quasi two-dimensional surface assuming unsteady conduction with constant thermal material properties, unsteady conduction with temperature-dependent material properties, transient conduction with standard wall convection, transient conduction with a specified wall temperature, steady-state radiation and reradiation. Exact solutions also exist for simple three-dimensional geometries with exclusively adiabatic and convective surface boundary conditions. Although the analytic solutions are provided in this report and discussed briefly for each case, the derivation and implementation details are omitted for brevity except where numerical error may be a notable factor.

## B. Unsteady Conduction with Constant Properties

The unsteady conduction problem requires Robin boundary conditions to specify the heat flux each side of the two-dimensional plate. The side defined as  $x = 0$  is arbitrarily selected as the surface to which there is a positive heat flux while the remaining three sides are assumed to be adiabatic as described by the following expressions:

$$-k \frac{\partial T}{\partial x} \Big|_{x=0} = \dot{q}'' \quad (130)$$

$$-k \frac{\partial T}{\partial x} \Big|_{y=0, x=L, y=L} = 0 \quad (131)$$

The initial condition can be set to any uniform temperature such that

$$T(x, t = 0) = T_0 \quad (132)$$

The exact solution in non-dimensional form is

$$\frac{T(x, t) - T_0}{\dot{q}'' L / k} = \frac{\alpha t}{L^2} + \frac{1}{3} - \frac{x}{L} + \frac{1}{2} \left( \frac{x}{L} \right)^2 - \frac{2}{\pi^2} \sum_{n=1}^{\infty} \frac{1}{n^2} \exp\left(-n^2 \pi^2 \frac{\alpha t}{L^2}\right) \cos\left(n\pi \frac{x}{L}\right) \quad (133)$$

where  $T_0$  is the initial temperature,  $L$  is the characteristic length of the plate and  $\alpha$  represents the thermal diffusivity of the material. The general procedure for calculating an infinite sum in any of the exact solutions is to continue adding terms until the absolute difference between consecutive values is within machine precision or  $1E-15$ . The material properties and other input parameters for the unsteady conduction problem are provided in Table ?? and are consistent for each of the cases presented in this report.

## C. Unsteady Conduction with Variable Properties

While the previous example was derived based on constant material properties, it is also possible to determine an exact solution wherein the specific heat and thermal conductivity are allowed to vary as a function of temperature to render a more physically realistic result. Despite evidence suggesting that both specific heat and thermal conductivity may actually have a quadratic thermal dependence, it is simply assumed for the purposes of this investigation that the material properties exhibit a linear relationship to temperature. Either way, *CATPISS* permits the user to specify each of the input material properties at any number of temperatures to achieve the desired level of accuracy.

$$k(T) = k_1 + \frac{k_2 - k_1}{T_2 - T_1} (T - T_1) \quad (134)$$

$$C_v(T) = C_{v,1} + \frac{C_{v,2} - C_{v,1}}{T_2 - T_1} (T - T_1) \quad (135)$$

$$\alpha = \frac{k_1}{\rho C_{v,1}} = \frac{k_2}{\rho C_{v,2}} = \frac{k(T)}{\rho C_v(T)} \quad (136)$$

The one-dimensional heat equation for temperature-dependent material properties is written as

$$\rho C_v \frac{\partial T}{\partial t} = \frac{\partial}{\partial x} \left( k \frac{\partial T}{\partial x} \right) \quad 0 \leq x \leq L \quad (137)$$

First, Kirchoff's transformation is applied to define a new variable  $\theta$ :

$$\theta = \frac{1}{k_{ref}} \int_{T_{ref}}^T k(\hat{T}) d\hat{T} \quad (138)$$

In a similar manner to the previous case, both heat flux boundary conditions and an initial temperature profile must be specified prior to searching for an exact solution:

$$-k \frac{\partial \theta}{\partial x} \Big|_{x=0} = \dot{q}'' \quad (139)$$

$$-k \frac{\partial \theta}{\partial x} \Big|_{y=0, x=L, y=L} = 0 \quad (140)$$



$$\theta(x, t = 0) = \theta_0 = \theta(T = T_0) \quad (141)$$

Several intermediate steps are taken to manipulate the original heat equation eventually leading to the result

$$\frac{\theta(x, t) - \theta_0}{\dot{q}'' L/k} = \frac{\alpha t}{L^2} + \frac{1}{3} - \frac{x}{L} + \frac{1}{2} \left( \frac{x}{L} \right)^2 - \frac{2}{\pi^2} \sum_{n=1}^{\infty} \frac{1}{n^2} \exp\left(-n^2 \pi^2 \frac{\alpha t}{L^2}\right) \cos\left(n\pi \frac{x}{L}\right) \quad (142)$$

It is interesting to note that this solution is in fact the same as for the constant property unsteady conduction problem with  $T$  replaced by  $\theta$ . Naturally, however, the results are quite different and deserve special consideration. As time advances the two cases tend to diverge since the medium's temperature is continually increasing.

#### D. Transient Conduction with Standard Convection

The problem of transient conduction with standard convection involves Robin boundary conditions such that one side of the plate is exposed to a fluid of temperature  $T_r$  and the remaining three sides are adiabatic:

$$-k \frac{\partial T}{\partial x} \Big|_{x=0} = H [T(t) - T_r] \quad (143)$$

$$-k \frac{\partial T}{\partial x} \Big|_{y=0, x=L, y=L} = 0 \quad (144)$$

Once again, the initial condition is uniform throughout the plate and set to a value denoted as  $T_0$ . The exact solution is

$$\frac{T(x, t) - T_r}{T_0 - T_r} = 2 \sum_{n=1}^{\infty} \left( \frac{\sin v_n}{v_n + \sin v_n \cos v_n} \right) \exp\left(\frac{-v_n^2 \alpha t}{L^2}\right) \cos\left(\frac{v_n x}{L}\right) \quad (145)$$

where  $v_n$  is the index eigenvalue that satisfies the equation

$$v_n \sin v_n = Bi \cos v_n \quad (146)$$

The parameter  $Bi$  in Eq. 146 is known as the Biot number and is defined as the ratio  $hL/k$ . In order to evaluate the terms of the infinite sum, it is first necessary to find the value of  $v_n$  that completes the implicit relationship for each index  $n$ . In general, this type of parameter is calculated using the Newton-Raphson method with an initial guess of  $Bi \cdot \pi/2$  and approximate periodicity of  $\pi$ . Implementation of the numerical technique does not appear to noticeably affect the efficiency of the exact solution routine which is written in the *FORTRAN* programming language. Moreover, the convergence tolerance between successive root estimations is set sufficiently high to avoid the propagation of error in the infinite sum.

#### E. Transient Conduction with Specified Temperature

The exact solution for transient conduction with a specified wall temperature is similar in form to the standard convection case although cast in terms of a freestream instead of recovery temperature  $T_{inf}$  and somewhat simpler. The boundary and initial conditions are set as

$$-k \frac{\partial T}{\partial x} \Big|_{x=0} = T_{\infty} \quad (147)$$

$$-k \frac{\partial T}{\partial x} \Big|_{y=0, x=L, y=L} = 0 \quad (148)$$

$$T(x, t = 0) = T_{\infty} \quad (149)$$

resulting in an analytic solution

$$\frac{T(x, t) - T_{\infty}}{T_0 - T_{\infty}} = 2 \sum_{n=1}^{\infty} \frac{(-1)^{n+1}}{v_n} \exp\left(\frac{-v_n^2 \alpha t}{L^2}\right) \cos\left(\frac{v_n x}{L}\right) \quad (150)$$

where  $v_n$  is now the index eigenvalue of the equation

$$\cos v_n = 0 \quad (151)$$

$$v_n = (2n - 1) \frac{\pi}{2} \quad (152)$$

The computation cost is reduced since the value of  $v_n$  is automatically known for all possible indices  $n$  without the need of numerical approximation.

## E. Steady-State Radiation and Reradiation

Both steady-state radiation and reradiation are governed by the total differential equation

$$\frac{d^2T}{dx^2} = 0 \quad (153)$$

For the case of radiation, the constant heat flux  $q$  is directed into the medium with an absorptivity  $\alpha$ :

$$q_{rad} = \alpha q \quad (154)$$

Reradiation implies that constant heat flux is exiting the medium with an emissivity  $\epsilon$  and background sink temperature  $T_b$  in addition to two parallel adiabatic sides:

$$-k \frac{dT}{dx} \Big|_{x=0} = \epsilon \sigma (T_{res}^4 - T_f^4) \quad (155)$$

$$-k \frac{dT}{dx} \Big|_{x=L} = T_b \quad (156)$$

$$-k \frac{dT}{dx} \Big|_{y=0, y=L} = 0 \quad (157)$$

The reradiation exact solution, therefore, is simply

$$\epsilon \sigma (T_{res}^4 - T_f^4) = \frac{k}{L} (T_f - T_b) \quad (158)$$

which is found via the Newton-Raphson approach to machine tolerance. A so-called unsteady reradiation verification case can be forged by extracting the evolution of surface temperature for unsteady conduction and assuming a linear relationship between emissivity and temperature to calculate the time history of sink temperature.

## G. Three-Dimensional Heat Equation on a Cube

In the case of transient conduction with standard convection, it is possible to extend the one-dimensional solution to a cubic geometry through the principle of superposition. The exact solution given in Eq. 145 is implemented in the  $x$ ,  $y$  and  $z$  directions independently to render the functions  $f(x)$ ,  $f(y)$  and  $f(z)$  which are then multiplied to give the non-dimensional solution at any point in the cube:

$$\frac{T(x, y, z, t) - T_r}{T_0 - T_r} = f(x) \cdot f(y) \cdot f(z) \quad (159)$$

It is also possible to specify different properties and heat flux conditions on each face of the cube, but for the purposes of this study opposite faces will be identical such that the center plane acts as an adiabatic surface to mimic the back of an ablating thermal protection material. The characteristic length  $L$  and convection coefficient  $h$  are permitted to vary between each direction.

## H. Three-Dimensional Heat Equation on a Cylinder

Transient conduction with standard convection on a cylinder is considerably more complicated in both the nature and implementation of the exact solution. First, several dimensionless parameters are defined

$$\frac{r}{r_0}, Bi = \frac{hr_0}{k}, Fo = \frac{\alpha t}{r_0^2} \quad (160)$$

where  $r$  is the cylinder radius,  $Bi$  is the Biot number as described previously and  $Fo$  is the Fourier number. Transforming the one-dimensional heat equation into cylindrical coordinates renders a Bessel-type partial differential equation with the solution

$$\frac{T(r, t) - T_\infty}{T_i - T_\infty} = \sum_{n=1}^{\infty} K_n J_0 \left( b_n \frac{r}{r_0} \right) \exp(-b_n^2 Fo) \quad (161)$$

As is the case with convection in one-dimension,  $b_n$  and  $K_n$  are eigenvalue index parameters but now depend on Bessel functions of the first kind  $J$ :

$$b_n J_1(b_n) = Bi J_0(b_n) \quad (162)$$

$$K_n = \frac{2Bi}{(b_n^2 + Bi^2) J_0(b_n)} \quad (163)$$

It should be noted that this analysis is only valid for long cylinders, or cylinders in which the length is much larger than the radius. Finite cylinders require an intersection of Eq. 161 with the non-dimensional temperature profile for a convective plate of half the characteristic length  $L$  (Eq. 159) as performed in the following manner:

$$\theta(r, x, t) = T(r, x, t) - T_\infty \quad (164)$$

$$\theta_i = T_i - T_\infty \quad (165)$$

$$\left[ \frac{\theta(r, x, t)}{\theta_i} \right]_{\text{finite cyl (L)}} = \left[ \frac{\theta(r, t)}{\theta_i} \right]_{\text{long cyl}} \cdot \left[ \frac{\theta(x, t)}{\theta_i} \right]_{\text{plate (L/2)}} \quad (166)$$

The main difficulty with this approach is calculating the value of various order Bessel functions at every point within the domain in addition to determining the eigenvalue index values with an inherently iterative numerical technique. One option commonly employed is to tabulate regular intervals of the Bessel functions and interpolate to the desired location. Although much more efficient than converging the infinite series definition of Bessel functions of the first kind, such a method greatly limits the applicability of the verification software to geometries of a similar size and simplicity. An optimized parallel processor code is a particularly attractive resolution to this issue.

## References

- <sup>1</sup> Adam Joseph Amar. Modeling of One-Dimensional Ablation with Porous Flow Using Finite Control Volume Procedure. Master's thesis, North Carolina State University, 2006.
- <sup>2</sup> Benjamin S. Kirk. *Adaptive Finite Element Simulation of Flow and Transport Applications on Parallel Computers*. PhD thesis, The University of Texas at Austin, May 2007.
- <sup>3</sup> Benjamin S. Kirk and Graham F. Carey. Development and Validation of a SUPG Finite Element Scheme for the Compressible Navier-Stokes Equations using a Modified Inviscid Flux Discretization. *International Journal for Numerical Methods in Fluids*, 57(3):265 – 293, 2008.